Optofluidic planar reactors for photocatalytic water treatment using solar energy

Lei Lei,[1] Ning Wang,[1] X. M. Zhang,[1,a)] Qidong Tai,[1] Din Ping Tsai,[2] and Helen L. W. Chan[1]
[1]*Department of Applied Physics, The Hong Kong Polytechnic University, Hong Kong, People's Republic of China*
[2]*Department of Physics, National Taiwan University, Taipei, Taiwan, Republic of China*

(Received 4 August 2010; accepted 31 August 2010; published online 30 December 2010)

Optofluidics may hold the key to greater success of photocatalytic water treatment. This is evidenced by our findings in this paper that the planar microfluidic reactor can overcome the limitations of mass transfer and photon transfer in the previous photocatalytic reactors and improve the photoreaction efficiency by more than 100 times. The microreactor has a planar chamber (5 cm $\times$ 1.8 cm $\times$ 100 μm) enclosed by two TiO_2-coated glass slides as the top cover and bottom substrate and a microstructured UV-cured NOA81 layer as the sealant and flow input/output. In experiment, the microreactor achieves 30% degradation of 3 ml $3\times10^{-5}M$ methylene blue within 5 min and shows a reaction rate constant two orders higher than the bulk reactor. Under optimized conditions, a reaction rate of 8% s^{-1} is achieved under solar irradiation. The average apparent quantum efficiency is found to be only 0.25%, but the effective apparent quantum efficiency reaches as high as 25%. Optofluidic reactors inherit the merits of microfluidics, such as large surface/volume ratio, easy flow control, and rapid fabrication and offer a promising prospect for large-volume photocatalytic water treatment. © *2010 American Institute of Physics.* [doi:10.1063/1.3491471]

I. INTRODUCTION

Recently, optofluidics technology has undergone a rapid development and has been explored for various applications, such as biomedical research, healthcare, pharmaceuticals, environmental protection, and homeland security. As a synergy of optics and microfluidics, optical elements such as waveguides, lasers, and plasmonics have been integrated into microfluidic devices. Novel functions and applications are enabled by exploiting the unique merits of microfluidics, such as laminar flow and large surface/volume ratio.[1–3] However, most of the reported work focused on laser generation and optical behaviors (light guiding, splitting, interference, etc.). The photocatalytic activity using microfluidic platform has not attracted due interest.

In fact, photocatalytic water treatment is naturally an optofluidic system since it bears the most important features of the optofluidics: light, fluid, and their interaction. Photocatalysis is a photoinduced chemical process based on the interaction between photons and semiconductor catalysts. When the semiconductor catalyst absorbs the photons that have an energy equal to or greater than the band-gap energy (3.2 eV for TiO_2), electron-hole pairs are created and dissociated into free electrons in the conduction band and holes in the valence band,[4] which can subsequently react with the chemicals and bioparticles by reduction and oxidation, and decompose them into harmless final products, such as CO_2, H_2O, and insoluble minerals. Due to this reason, photocatalysis has been extensively applied to water pollution treatment,[4] air purification,[5] disinfection,[6]

a)Author to whom correspondence should be addressed. Electronic mail: apzhang@inet.polyu.edu.hk. FAX: +852-2333-7629. Tel.: +852-3400-3258.

self-cleaning, and water splitting.[7] However, industrial applications are now still in the infancy as limited by the low photocatalytic efficiency and the difficulty to scale up from laboratory proof-of-concept to large-volume production.

The photocatalytic efficiency is mainly determined by the illumination efficiency and the contact between the activated catalyst and the reagents.[8] The former is also called *photon transfer efficiency* and is affected by the illustrated surface per unit liquid volume (related to the illustration area and the surface/volume ratio) and the effective incident power density (related to the power density, the absorption, and the wavelength of incidence). The latter is sometimes called *mass transfer efficiency* and reflects how easy the reagents in the liquid are moved to the catalyst surface (related to the catalysis surface area per unit volume) and how fast the reacted products are removed (related to the diffusion, stirring, and flow rate).

Microfluidics has a natural synergy with photocatalysis since its inherent large surface/volume ratio could drastically enhance the photon transfer efficiency and the mass transfer efficiency. Indeed, several microfluidic photocatalytic reactors have been demonstrated and showed high reaction efficiency and good controllability compared to the conventional plate and slurry reactors.[9–13] However, the previous microfluidic reactors mostly utilized microchannel-based design and suffered from reduced light absorption area, limited volume of reactants, and low throughput. Besides, they relied on expensive and time-consuming fabrication processes, such as direct laser-writing,[11] dry and wet etching,[9–13] and thermal bonding,[9–13] and thus impeded the prospect of industrialization. In addition, most of the demonstrated work made use of UV lamps as the light source, the comparatively high cost associated with the consumption of electricity constitutes one of the major drawbacks for the rapid commercialization of photocatalytic water treatment.[14] Solar-powered photocatalysis presents to be the most viable route to energy conservation and low-cost production. Different types of large-scale solar-powered reactors have been tested in laboratory and field.[14] For instance, the thin-film fixed-bed reactor design has demonstrated with high efficiency of solar energy utilization; thanks to its planar structure.[15] Nevertheless, miniaturized version has yet to investigate.

This work will demonstrate a planar microfluidic photocatalytic reactor for water treatment using solar energy, which attempts to combine the merits of the microfluidics and planar reactors while circumventing their problems. The device is formed by an UV curable resin NOA81 (Norland Optical Adhesive) and TiO_2 film coated glasses, making the whole fabrication process rapid and low cost. To study the feasibility of solar-powered photocatalytic water treatment, methylene blue will be used as the organic model and its photodegradation will be examined under solar irradiation. Influences of the reactor parameters (e.g., film preparation methods, thickness of TiO_2 films, and flow rate) and characterization of photocatalytic efficiency will be studied in detail.

II. EXPERIMENTAL DETAILS

A. Device design

In order to enlarge the light absorption area and keep the inherent merit of large surface/volume ratio of microreactors, a planar microfluidic reactor is designed as illustrated in Fig. 1. For simplicity, the planar microfluidic reactor is called *microreactor* hereafter. The microreactor has a rectangular reaction chamber, which is constructed by two porous TiO_2-coated glasses as the top cover and bottom substrate, and a 100-μm-thick UV curable adhesive layer (NOA81, Norland) as the spacer and sealant. The dimensions of the reaction chamber are $5\ \text{cm} \times 1.8\ \text{cm} \times 100\ \mu\text{m} = 90\ \mu\text{l}$ and the TiO_2 films on the glasses have the same surface area with the reaction chamber. Two syringe needles are used as the inlet and outlet for solution injection and collection. Between the reaction chamber and inlet/outlet, tree-branch shaped microchannels (50 μm high) are adopted to ensure a uniform filling of the solution over the whole reaction chamber and thus a maximum contact of the reagents with the TiO_2 films.

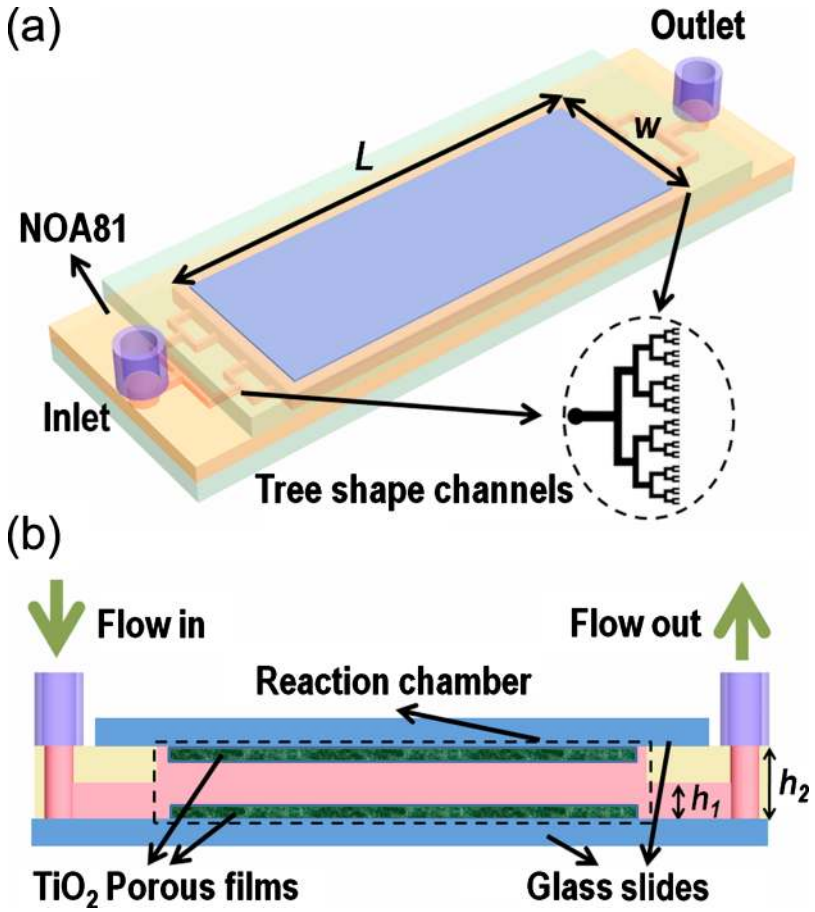

FIG. 1. (a) Schematic and (b) cross-sectional view of the photocatalytic microfluidic reactor. The device is constructed by two TiO_2-coated glasses separated by a thin layer of microstructured UV-cured NOA81. Tree-branch shaped microchannels are used to ensure that the solution uniformly fills the whole reaction chamber and have maximum contact with the TiO_2 films. The length and width of the reaction chamber are $L=5$ cm and $W=1.8$ cm, respectively. The TiO_2 films have the same surface area as the reaction chamber. The heights of the microchannels and the reaction chamber are $h_1=50$ μm and $h_2=100$ μm, respectively.

B. Preparation of porous TiO_2 films

The porous TiO_2 films were prepared by sol-gel method,[16] which included two stages: the preparation of the TiO_2 colloid and the creation of porous TiO_2 film on the glass slide. On the first stage, 12 g TiO_2 powders (Degussa P25, a mixture of ~30% rutile and 70% anatase, the mean size of primary particles to be about 25 nm) were slowly dispersed in 120 ml water, which contained acetylacetone (0.4 ml, Sigma-Aldrich) to prevent aggregation of the particles with the assistance of magnetic stirring. After the powder had been well dispersed, a detergent (0.2 ml Triton X-100, Sigma-Aldrich) was added to facilitate the spreading of the colloid on the substrate. Finally, 2.4 g polyethylene glycol (Sigma-Aldrich) was added into the solution under continuous stirring over one whole night.

On the second stage, a glass slide was covered on four edges with adhesive tapes (about 40 μm thick) to control the thickness of the TiO_2 film and to protect the noncoated areas. As a result, a region of 5 cm $\times$ 1.8 cm at the center of the glass was exposed. Then the colloid (10 μl) was applied to one edge of the exposed region of glass and was distributed by sliding a glass rod over the tape-covered edges. With the tapes as the spacer, a uniform layer of colloid was obtained in the exposed region. After air drying at 80 °C, the tapes were removed and the glass slide was calcined for 2 h at 500 °C in air. The resultant film was observed using scanning electron micro-

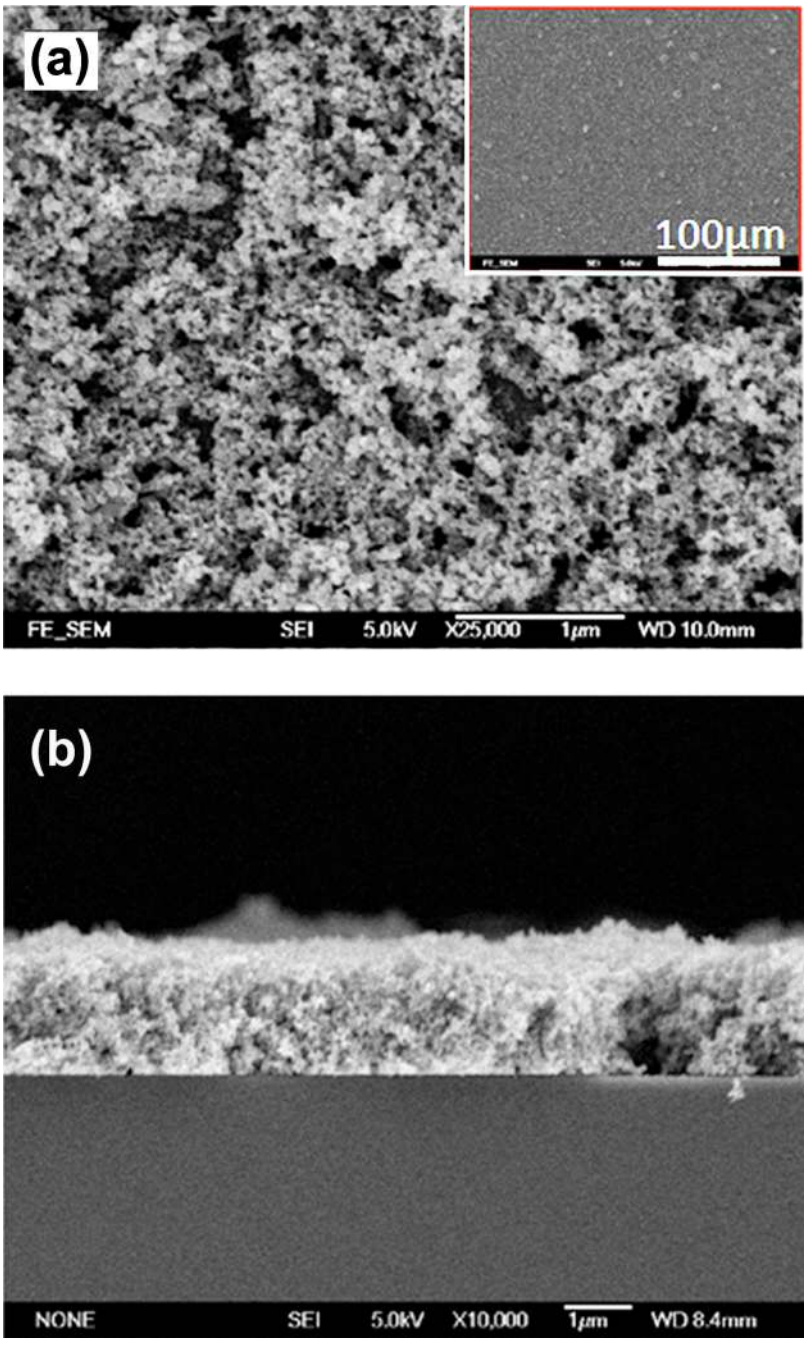

FIG. 2. Scanning electron micrographs showing the porous structure of the fabricated TiO_2 film. (a) Top view of the film: the submicron porous structures are beneficial as they increase the contact area between the reagents and TiO_2 and thus improve the photocatalytic efficiency. The inset shows the good homogeneity of the film. (b) Cross-sectional view of the film: the film is about 2 μm thick and shows a good homogeneity in the depth direction.

scope. Figure 2(a) shows the close-up of the film, with an inset showing a much larger region. Figure 2(b) shows the cross-section of the film. It can be observed that the resultant TiO_2 has submicron porous structures and good homogeneity. The film thickness is 2 μm and can be varied by changing the colloid concentration.

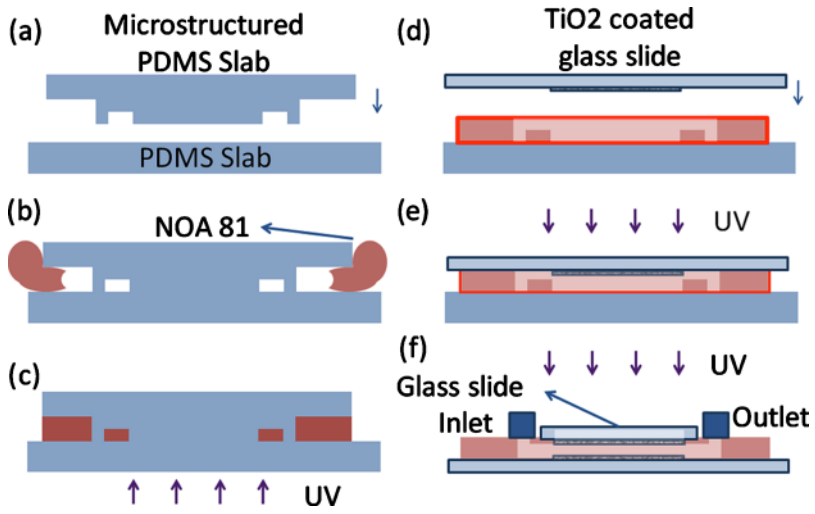

FIG. 3. Process flow of the device fabrication and integration. Microstructured PDMS slab is replicated from the SU-8 mold in advance. (a) The microstructured slab is attached to a planar PDMS slab. (b) Liquid NOA81 is applied to fill the space between the two PDMS slabs by capillary force. (c) The NOA81 is partially cured by the UV light. (d) The microstructured PDMS slab is peeled off and the NOA81 layer is bonded to a TiO_2-coated glass slide. (e) The other glass slide is bonded by UV exposure. (f) Two syringe needles are connected to the inlet and outlet using adhesive.

C. Microfluidic device fabrication

Polydimethysiloxane (PDMS) is most popular for microfluidic devices because of its celebrated physical and chemical properties. However, it is not a good candidate for this microreactor because its elastic modulus is too low to support a chamber with high width/height ratio (collapse otherwise) and a thin layer of PDMS can be broken easily. NOA81 is chosen since it has high elastic modulus (typically 1 GPa, three orders of magnitude higher than PDMS) and can be easily bonded to the glass by UV exposure.[17] In addition, NOA81 has a better resistance to swelling by solvents than PDMS and allows the replication of submicron features.

Standard UV lithography was used to fabricate the master mold for the microreactor. First, negative photoresist SU-8 50 was spin coated (2500 rpm, 60 s, and 50 μm) onto a silicon wafer substrate and baked. Reaction chamber and inlet/outlet were then patterned with a mask. The process was repeated and the microchannels were also patterned with another mask. As a result, the SU-8 master was obtained. After the evaporation of trimethylchlorosilane on the surface of the SU-8 master, a prepolymer solution of PDMS in a 10:1 mixture ratio was poured on and cured at 80 °C for 1 h. Finally, the cured PMDS slab was then peeled off and ready for making the microreactor.

The process flow for replicating the structures to the NOA81 layer and for eventually forming the microreactor is shown in Fig. 3. First, the microstructured PDMS slab was attached to a planar PDMS slab [see Fig. 3(a)]. Then, drops of liquid NOA81 were then applied to the edges of the PDMS slab so as to fill the space between the two PDMS slabs by capillary force [see Fig. 3(b)]. Next, UV exposure (10 mW/cm^2 and 20 s) was applied to cure the NOA81 [see Fig. 3(c)]. Since oxygen inhibited the free-radical polymerization of liquid NOA81,[17] the PDMS's permeability to gas ensured that an ultrathin superficial layer of NOA81 liquid remained uncured in close proximity to each PDMS surface, although the central part of NOA81 had already been hardened. After that the microstructured PDMS slab was gently peeled and the NOA81 layer was pressed onto a porous TiO_2 film coated glass slide [bottom glass, see Fig. 3(d)]. Subsequent UV exposure (10 mW/cm^2 and 8 s) cured the remaining liquid NOA81 layer and bonded them firmly. By then there still remained an uncured thin layer of NOA81 on the planar PDMS slab side. By the same method, it was bounded to another porous TiO_2 film coated glass slide [cover glass, see Fig. 3(e)]. Finally, two syringe tips were connected to the inlet and outlet using adhesive [see Fig. 3(f)]. The

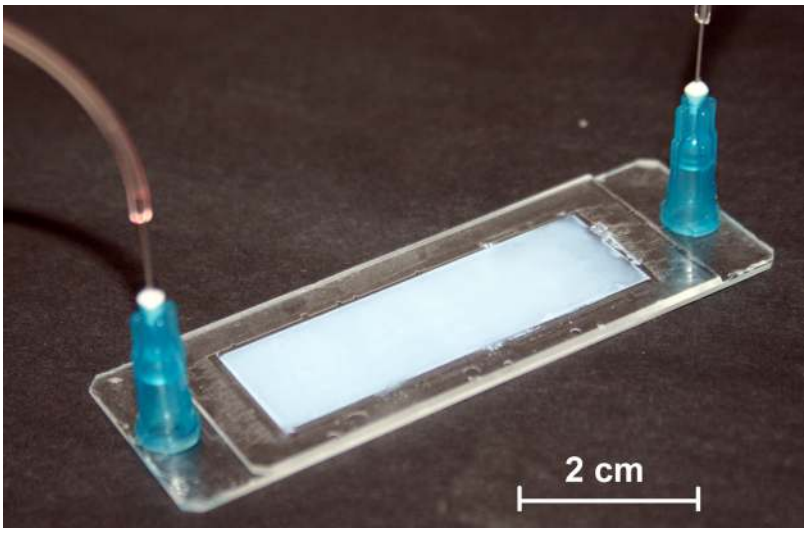

FIG. 4. Photograph of the fabricated planar microfluidic photocatalytic reactor.

process was easy and low cost. It took less than 5 min to run the whole procedures to make a microreactor from the master mold. A photograph of the fabricated device is shown in Fig. 4. It has a footprint of 7.6 cm $\times$ 2.5 cm and encloses a microreactor chamber with the dimensions of 5 cm $\times$ 1.8 cm $\times$ 100 μm (volume 90 μl).

D. Experimental setup for methylene blue degradation

The photocatalytic reaction was under 100 mW/cm^2 solar irradiation by a solar simulator equipped with an AM 1.5G filter (Newport 91160, 150w). Methylene blue (MB) (Sigma-Aldrich) solution was introduced into the device by a syringe pump (TS2-60, Longer). The degraded MB solutions were collected from the outlet and their absorption spectra were analyzed by a UV-visible spectrophotometer (UV-2550, Shimadzu).

III. RESULTS AND DISCUSSIONS

A. Enhancement of photocatalytic efficiency by microfluidic reactor

To quantify the enhancement of photocatalytic efficiency by using the microreactor, a bulk container having the same porous TiO_2 film was used as the reference. The bulk container was formed by cutting a 5×1.8 cm^2 square hole at the center of a 7-mm-thick PDMS slab and by then attaching it onto a TiO_2-film coated glass slide. After the attachment, the TiO_2 film lay on the bottom of the bulk container. The bulk container can hold up to 6.3 ml solution. It is noted that for fair comparison, the microreactor has only one porous TiO_2 film on the bottom glass while the top glass is just a plain glass slide. In this way, the microreactor and the bulk container have the same TiO_2 surface. Microreactor without TiO_2 was also tested to verify the effect of the TiO_2 presence.

To study the photocatalytic degradation, 3 ml MB solution ($3 \times 10^{-5} M$ and $p\mathrm{H} \sim 7$) was added into the bulk container and then irradiated under the solar simulator (100 mW/cm^2). The absorption spectra of the photodegraded solutions after 20 min, 40 min, and 1 h of exposure in the container were analyzed. The same amount of solution was also introduced into the microreactor by a syringe pump and irradiated under the same solar light. The photodegraded solutions under different evacuation times, such as 5, 15, and 30 min in the reactor with and without TiO_2 were also examined. Here the evacuation time refers to the overall time needed to flow all the solution from the inlet to the outlet. Therefore, the flow rates corresponding to the evacuation times of 5, 15, and 30 min are 600, 200, and 100 μl/min, respectively. One of the main differences is that in the bulk container the 3 ml solution was constantly exposed to the solar light over the whole

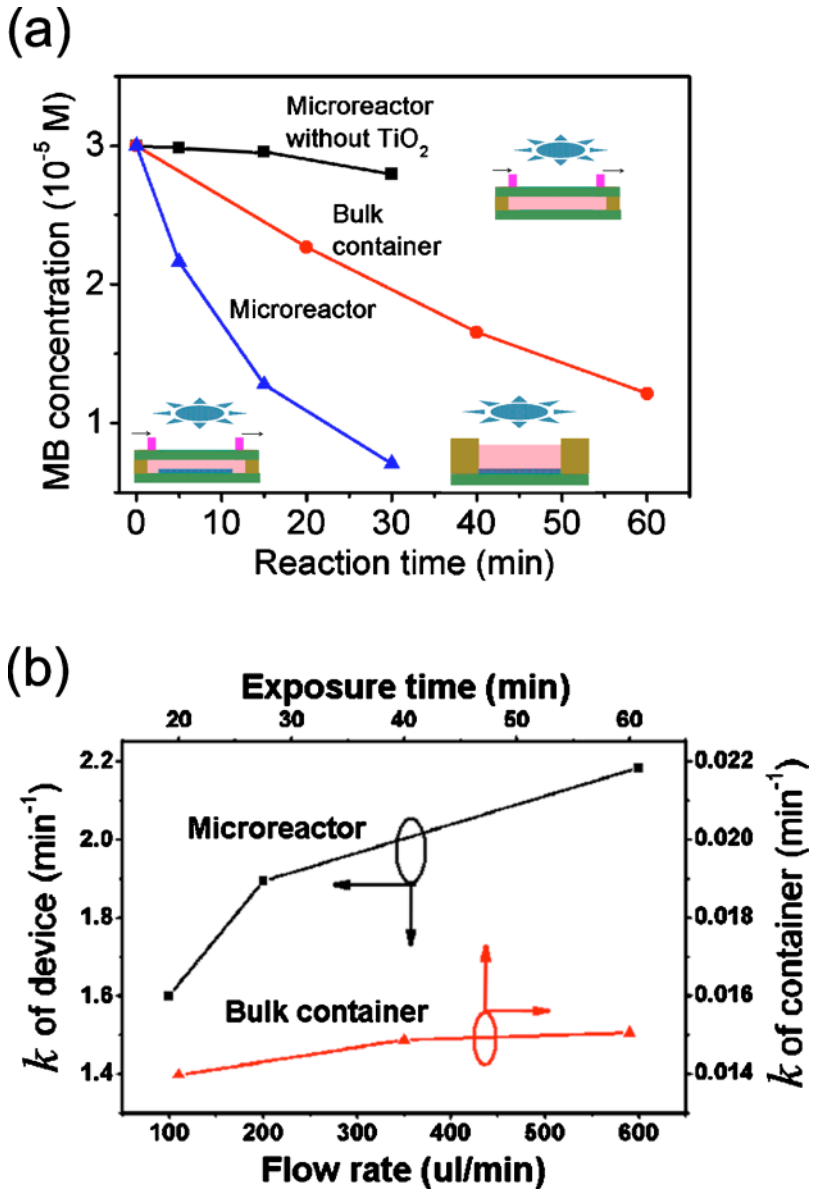

FIG. 5. (a) Comparison of the photocatalytic reaction efficiencies. The microreactor shows much higher reaction efficiency than the container. For further comparison, the microreactor without TiO_2 is also tested and its reaction is found negligible. (b) The reaction rate constant of the microreactor is more than 100 times higher than that of the bulk container and presents to increase with the flow rate of the solution.

exposure time, whereas in the microreactor the residence time (i.e., the effective exposure time) of the solution is much shorter than the evacuation time. For instance, the residence time is only 0.15 min for the evacuation time of 5 min.

From the Beer–Lambert law,

$$\text{absorbance} = \varepsilon c l, \tag{1}$$

where ε is the molar absorptivity, l is the optical path, and c is the concentration. The degradation can be evaluated by monitoring the absorbance change at 664 nm wavelength of MB solutions before and after being degraded.[12]

Figure 5(a) plots the MB concentration changes over the reaction time for the bulk container

and the microreactor with and without TiO_2. Here the reaction time refers to the exposure time for the bulk container but the evacuation time for the microreactor. It is seen that the microreactor with TiO_2 exhibited faster decrease of MB concentration than the bulk container. For example, a degradation of 30% of MB (from the initial $3\times10^{-5}M$ to the level of $2\times10^{-5}M$) took 5 min in the microreactor but more than 20 min in the bulk container. However, the photoreaction in the microreactor without TiO_2 is negligible, which validates the significant effect of TiO_2 presence on the reaction efficiency.

In data analysis, the reaction rate constant can be deduced from the degradation in the reactor[18]

$$k = -\frac{\ln(1-x)}{t}, \tag{2}$$

where k represents the reaction rate constant, x is the degradation percentage of the reactants, and t is the effective reaction time. Using this equation, the reaction rate constants of the microreactor and the bulk container can be calculated and compared. The results are plotted in Fig. 5(b). For the microreactor the reaction rate constant is plotted against the flow rate, whereas for the bulk container it is against the exposure time. It can be read from the curves that the reaction rate constant k of the microreactor ranges from 1.6 to 2.2 min^{-1} and that of the bulk container is from 0.014 to 0.015 min^{-1}. The value of the microreactor is more than two orders higher than that of the bulk container. This proves that microfluidics indeed brings in remarkable improvement of reaction rate to the photocatalytic reactors.

Such improvement can be explained by considering the mass transfer efficiency. The reaction rate constant is determined by two factors: the intrinsic reaction rate and the external mass transfer efficiency of MB from the liquid to the TiO_2 film surface,[18]

$$\frac{1}{k} = \frac{1}{k_i K} + \frac{1}{k_m \alpha_v}, \tag{3}$$

where k_i is the intrinsic reaction rate constant, K is the Langmuir adsorption coefficient, k_m is the mass transfer coefficient, and α_v is the ratio of the TiO_2 surface to the reactor volume. The first term in Eq. (3) reflects the influence of the intrinsic reaction and is independent of the flow rate and the reactor volume. The second term of Eq. (3) is the contribution of the external mass transfer. In the bulk container, the mass transfer presents to be the main limitation. Nevertheless, in the microfluidic reactors, k_m and α_v are very high because of its inherent microscale and large surface/volume ratio. As a result, the reaction efficiency is only limited by the intrinsic kinetics. This is one of the key merits of using microfluidics for photocatalytic reaction. It is also observed from Fig. 5(b) that the rate constant increases with the flow rate. Detailed study and explanation will be presented in Sec. III C.

B. Effect of TiO_2 film thickness

In our final microreactor, two TiO_2 films are utilized, one is at the bottom glass while the other on the top glass. For simplicity, they are named as bottom and top films, respectively. Their thicknesses would affect the reaction efficiency in different ways. For the bottom film, the effective surface area would increase with the thickness due to the porous morphology of the TiO_2 film, particularly when the film is very thin. As a result, the reaction efficiency is expected to increase with the TiO_2 thickness. However, when the film becomes very thick, the pores in the inner part are not exposed to the solution or the light, and thus do not contribute to the photoreactivity. As a result, there exists a thickness at which the reaction efficiency starts to saturate. This conclusion would apply equally to the reactors with only one TiO_2 film (such as the bulk container and the microfluidic reactor having only one glass coated with TiO_2). Nevertheless, it is very different for the top film. On one hand, the top film absorbs some light for photocatalysis. On the other hand, it has to transmit some light to the bottom film for further photocatalysis. Too thin a top film would

have low contribution to the overall photoreactivity, but too thick a top film would block the light and render the bottom film useless. There exists an optimal thickness for the top film.

In experiment study, porous TiO_2 films with different thicknesses (0.5, 1, 1.3, and 2 μm) were prepared using the TiO_2 P25 aqueous solutions with different concentrations (2%, 4%, 6%, and 10%, respectively) following the procedures as discussed in Sec. II B. The obtained film thickness as a function of the TiO_2 concentration is plotted in the inset of Fig. 6(a), showing roughly a linear relationship. Figure 6(a) shows the transmission spectra (over the wavelength of 250–450 nm) of the films under the solar irradiation. The transmission intensities decrease with the thicknesses of the films and approach to zero when the thickness of the film goes up to 2 μm. In other words, a 2 μm TiO_2 film would absorb almost all the light.

Reaction efficiencies of the TiO_2 films with different thicknesses were compared using the bulk container configuration. The degradation percentages of 3 ml MB solution (concentration of $3\times10^{-5}M$) after 30 min exposure time were measured to indicate the reaction efficiencies. Here the degradation percentage refers to the percentage of the initial MB being degraded during the exposure time. The results are shown in Fig. 6(b). The degradation percentage increases rapidly when the thickness goes from 0.5 to 1 μm, and tends to saturate at thickness larger than 1 μm. This matches well with the above prediction. For this reason, the final microreactor is chosen to use a 2-μm-thick TiO_2 film on the bottom glass.

The influence of the top film thickness was determined using four microreactors that had the same bottom film thickness of 2 μm but different top film thicknesses (0.5, 1, 1.3, and 2 μm, respectively). The reaction efficiencies were obtained by measuring the degradation of MB solutions at a flow rate of 600 μl/min. The results are plotted in Fig. 6(c). It is found that the thickness of 1 μm is the best choice for the top film. The following experiments will be done with this optimized device.

C. Effect of flow rate

The influence of the flow rate on the photocatalytic reaction efficiency was also studied. The flow rate is related to the effective residence time of the MB solution in the reaction chamber by the relationship (effective residence time)=(chamber volume)/(flow rate). Here the chamber volume is 90 μl as already given above. The experimental results are plotted in Fig. 7. The degradation percentage increases with the effective residence time and reaches 94% at 36 s (corresponding to the flow rate 150 μl/min). This is easy to understand because the longer the residence time is, the more the photoreaction occurs. However, it is shown in Fig. 7 that the reaction rate actually decreases with longer residence time (equivalently, it increases with the flow rate). For instance, it is as high as 8%/s at the effective residence time of 6 s (corresponding to the flow rate 900 μl/min) and drops to only 2.6%/s at the effective residence time of 36 s. To further illustrate such behavior, the reaction rate constant k as a function of the flow rate is plotted in the inset of Fig. 7. It is seen clearly that the reaction rate constant gradually increases with higher flow rate. The reason for this behavior is not that straightforward but can be explained by considering the mass transfer efficiency and the oxygen availability during the reaction. The photon transfer situation is almost invariant during the variation of the flow rate.

In this device, the illuminated specific surface/volume of the photocatalyst in contact with the reactant can be calculated to be $r=2(LW)/(LWh_2)=20\,000$ m^{-1}, where L, W, and h_2 are the length, width, and height of the reaction chamber, respectively [see Fig. 1(a)]. The value of 20 000 m^{-1} is just the lower limit. The actual value should be much larger due to the porous morphology of the TiO_2 film. Such a high surface/volume ratio would significantly improve the mass transfer efficiency. To reach a quantitative estimation, detailed photoreaction kinetics has to be considered. According to the previous studies,[12,13] the heterogeneous Damköhler number Da_{II}, which represents the ratio of the heterogeneous reaction rate at the catalyst surfaces to the diffusion from the bulk solution toward the catalyst surfaces, can reflect the mass transfer limitation in the microreactors. The Da_{II} number of our device is calculated to be 0.003 using the equations and parameters from Ref. 12. When the Da_{II} number is less than 0.1, the reaction rate is dominated by the intrinsic kinetics of the photoreactions, which indicates that there is no mass transfer limitation

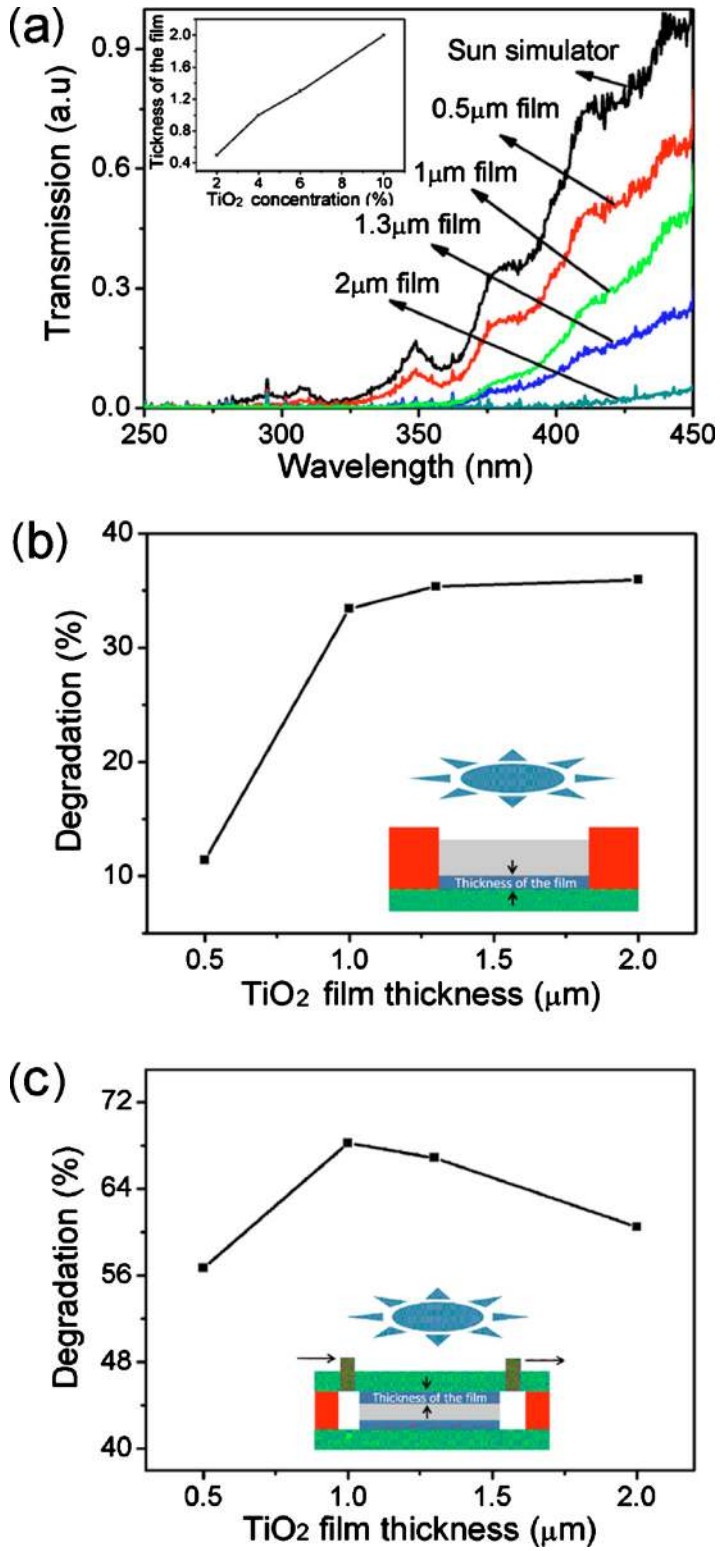

FIG. 6. (a) Transmission spectra (in the UV region) of the TiO_2 porous films with different thicknesses under the irradiation of solar simulator. The inset shows the relationship between the thickness of the obtained TiO_2 porous film and the concentration of the TiO_2 aqueous solution using the sol-gel method. (b) Degradation percentage as a function of the TiO_2 film thicknesses using the bulk container. (c) Degradation percentage as a function of the TiO_2 film thicknesses on the top glass using the microreactor. The TiO_2 film thickness on the bottom glass is kept at 2 μm.

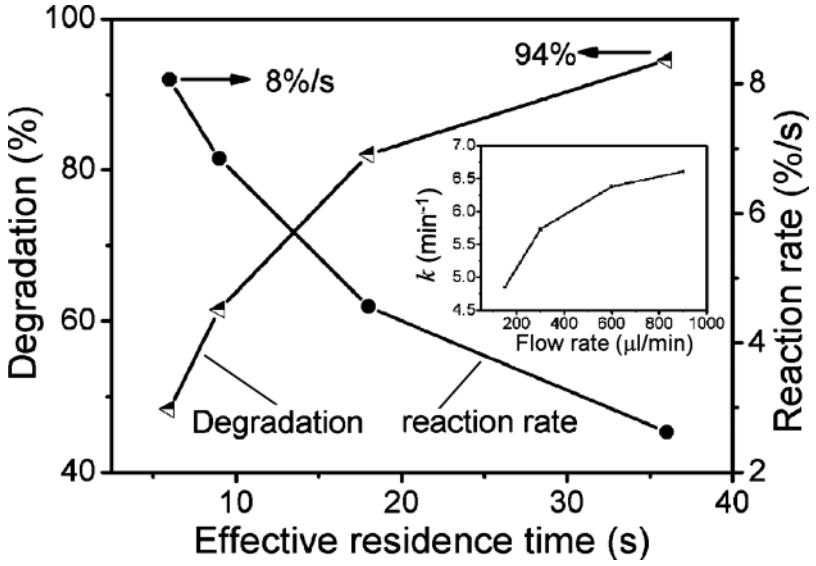

FIG. 7. Degradation percentage and reaction rate with respect to different effective residence times of the methylene blue solution in the reaction chamber. The degradation percentage increases with the effective residence time, whereas the reaction rate decreases. The inset shows that the reaction rate constant increases with the flow rate.

for the photocatalytic reaction in this microreactor. The calculation also indicates that the height of the reaction chamber should not exceed 570 μm to avoid the adverse effect of the mass transfer limitation.

Oxygen availability is crucial to the MB photocatalytic degradation, which can be seen by the reaction equation

$$C_6H_{18}N_3SCl + 25.5O_2 \xrightarrow{TiO_2+h\nu\geq 3.2\ eV} HCl + H_2SO_4 + 3HNO_3 + 16CO_2 + 6H_2O. \quad (4)$$

According to this equation, the degradation of $3\times10^{-5}M$ MB solution needs $7.5\times10^{-4}M$ oxygen, which is three times higher than the dissolved oxygen at room temperature and atmospheric pressure. At low flow rate, the consumption of oxygen would cause a deficiency of oxygen and thus a reduction of the reaction efficiency. In contrast, a high flow rate helps refuel the photoreaction using the dissolved oxygen in newly arrived solution. The deficiency of oxygen is supposed to be the main reason for the decrease of reaction efficiency at lower flow rate. To solve this problem, a recycle design[18] or an addition of small amount of H_2O_2 (Ref. 19) can be used.

D. Light utilization efficiency

Quantum efficiency can be used to evaluate the efficiency of the photocatalytic reactor. It is defined as a number of molecules N_{mol} reacted relative to the number of quanta N_{photon} absorbed by the photocatalyst or reactants,

$$\Phi = \frac{N_{mol}}{N_{photon}}. \quad (5)$$

Normally, the quantum efficiency is characterized using a monochromatic light. However, we will study the average quantum efficiency for the whole activating region ($\geq$3.2 eV or $\leq$387.5 nm) of the solar irradiation. Besides, it should be mentioned that the total energy arrived on the device is not just absorbed by the catalyst and reactants but is also lost by diffraction, scattering, and reflection of the device. So the quantum efficiency here is not the actual quantum efficiency but the apparent quantum efficiency.

Calculated from the solar irradiation under AM 1.5 condition,[20] the number of the activating photons arrives at the TiO_2 films is 5.887×10^{16} photons/s. The maximum reaction rate of 8%/s corresponds to the decomposition of 1.45×10^{14} molecules/s of MB. In this case, the average quantum efficiency is 0.25%. However, the total mineralization of one MB molecule needs 102 oxidizing equivalents produced by the photoelectrochemical reactions.[12] If we take this into account, the effective apparent quantum efficiency should be as high as 25%.

It should be pointed out that the energy of activating irradiation for the TiO_2-based photocatalysis is only 3.65% of the whole solar irradiation.[20] The total light utilization efficiency is still very low in this case. Fortunately, several methods are being studied for visible light photocatalysis, such as doping in TiO_2 (Ref. 21) and plasmonic sensitization.[22] Further work will be done to improve the light utilization efficiency using these modified materials.

IV. CONCLUSIONS

A planar photocatalysis microfluidic reactor was designed and characterized with methylene blue photodegradation under solar irradiation for performance evaluation. A low-cost and simple method was used for the device fabrication. Experiments proved that much higher reaction efficiency could be achieved by this microreactor as compared to the bulk container. Different factors, such as the TiO_2 film thickness and the flow rate, were investigated to optimize the microreactor performance. 8% s^{-1} reaction rate under solar irradiation was achieved at the flow rate of 900 μl/min. The apparent average quantum efficiency of device under the whole activating solar irradiation ($\geq$3.2 eV) was found to be 0.25%. The main limitations of the device are the oxygen deficiency in the reactants and the low solar spectrum sensitivity. The subsequent research work will focus on increasing the oxygen availability in the reaction chamber and improving the visible light sensitivity of the photocatalyst.

ACKNOWLEDGMENTS

This work was supported by The Hong Kong Polytechnic University through Grant Nos. 1-ZV5K, A-PD1S, and G-YH81.

[1] D. Psaltis, S. R. Quake, and C. H. Yang, Nature (London) **442**, 381 (2006).
[2] C. Monat, P. Domachuk, and B. J. Eggleton, Nat. Photonics **1**, 106 (2007).
[3] A. Q. Liu, H. J. Huang, L. K. Chin, Y. F. YU, and X. C. Li, Anal. Bioanal. Chem. **391**, 2443 (2008).
[4] J. M. Herrmann, Catal. Today **53**, 115 (1999).
[5] J. Mo, Y. Zhang, Q. Xu, J. J. Lamson, and R. Zhao, Atmos. Environ. **43**, 2229 (2009).
[6] C. Wei, W. Lin, Z. Zainal, N. E. Williams, K. Zhu, A. P. Krurlc, R. L. Smith, and K. Rajeshwar, Environ. Sci. Technol. **28**, 934 (1994).
[7] Z. Zou, J. Ye, K. Sayama, and H. Arakawa, Nature (London) **414**, 625 (2001).
[8] T. Van Gerven, G. Mul, J. Moulijn, and A. Stankiewicz, Chem. Eng. Process. **46**, 781 (2007).
[9] H. Lu, M. A. Schmidt, and K. F. Jensen, Lab Chip **1**, 22 (2001).
[10] G. Takei, T. Kitamori, and H. B. Kim, Catal. Commun. **6**, 357 (2005).
[11] R. C. R. Wootton, R. Fortt, and A. J. de Mello, Org. Process Res. Dev. **6**, 187 (2002).
[12] H. Lindstrom, R. Wootton, and A. Iles, AIChE J. **53**, 695 (2007).
[13] R. Gorges, S. Meyer, and G. Kreisel, J. Photochem. Photobiol., A **167**, 95 (2004).
[14] D. Bahnemann, Sol. Energy **77**, 445 (2004).
[15] R. Goslich, R. Dillert, and D. W. Bahnemann, Water Sci. Technol. **35**, 137 (1997).
[16] M. K. Nazeeruddin, A. Kay, L. Rodicio, R. Humpbry-Baker, E. Miiller, P. Liska, N. Vlachopoulos, and M. Gratzel, J. Am. Chem. Soc. **115**, 6382 (1993).
[17] D. Bartolo, G. Degré, P. Nghe, and V. Studer, Lab Chip **8**, 274 (2008).
[18] H. Lin and K. T. Valsaraj, J. Appl. Electrochem. **35**, 699 (2005).
[19] P. Nalini Vi jaya Laxmi, P. Saritha, N. Rambabu, V. Himabindu, and Y. Anjaneyulu, J. Hazard. Mater. **174**, 151 (2010).
[20] R. E. Bird, R. L. Hulstrom, and L. J. Lewis, Sol. Energy **30**, 563 (1983).
[21] R. Asahi, T. Morikawa, T. Ohwaki, K. Aoki, and Y. Taga, Science **293**, 269 (2001).
[22] E. Kowalska, O. O. P. Mahaney, R. Abe, and B. Ohtani, Phys. Chem. Chem. Phys. **12**, 2344 (2010).